BIOCHEMISTRY

Targeting oncoproteins with a positive selection assay for protein degraders

Vidyasagar Koduri[1]*, Leslie Duplaquet[1]*, Benjamin L. Lampson[1], Adam C. Wang[1], Amin H. Sabet[1], Mette Ishoey[1], Joshiawa Paulk[1†], Mingxing Teng[2,3], Isaac S. Harris[4,5‡], Jennifer E. Endress[4,5§], Xiaoxi Liu[2,6], Ethan Dasilva[2,6], Joao A. Paulo[5], Kimberly J. Briggs[1‖], John G. Doench[7], Christopher J. Ott[1], Tinghu Zhang[2,3], Katherine A. Donovan[2,3], Eric S. Fischer[2,3], Steven P. Gygi[5], Nathanael S. Gray[2,3], James Bradner[8], Jeffrey A. Medin[9], Sara J. Buhrlage[2,6], Matthew G. Oser[1,10,11¶], William G. Kaelin Jr.[1,11,12¶]

Most intracellular proteins lack hydrophobic pockets suitable for altering their function with drug-like small molecules. Recent studies indicate that some undruggable proteins can be targeted by compounds that can degrade them. For example, thalidomide-like drugs (IMiDs) degrade the critical multiple myeloma transcription factors IKZF1 and IKZF3 by recruiting them to the cereblon E3 ubiquitin ligase. Current loss of signal ("down") assays for identifying degraders often exhibit poor signal-to-noise ratios, narrow dynamic ranges, and false positives from compounds that nonspecifically suppress transcription or translation. Here, we describe a gain of signal ("up") assay for degraders. In arrayed chemical screens, we identified novel IMiD-like IKZF1 degraders and Spautin-1, which, unlike the IMiDs, degrades IKZF1 in a cereblon-independent manner. In a pooled CRISPR-Cas9–based screen, we found that CDK2 regulates the abundance of the ASCL1 oncogenic transcription factor. This methodology should facilitate the identification of drugs that directly or indirectly degrade undruggable proteins.

INTRODUCTION

Many protein targets linked to human diseases cannot be addressed with antibodies because they are intracellular and cannot be addressed with conventional small-molecule drugs because they lack suitable drug-binding pockets that influence their function. The recent discovery that thalidomide-like immunomodulatory drugs (IMiDs) kill multiple myeloma cells by reprogramming the cereblon ubiquitin ligase complex to target two otherwise undruggable transcription factors (IKZF1 and IKZF3) for destruction has galvanized interest in finding other small-molecule protein degraders (*1*, *2*). Protein stability is a highly regulated process, and there are many ways, in addition to ubiquitin ligase reprogramming, that a small molecule could alter protein stability. For example, a small molecule might alter a post-translational modification that normally dictates the stability of the protein of interest (POI) or could inhibit a deubiquitinating enzyme that normally removes destabilizing ubiquitin chains from that protein.

Despite these advances, there remains a great need for improved screening approaches to accelerate the discovery of degraders. Conventional assays for protein degraders that measure protein loss (a "down assay") can be confounded if transcription or translation are likewise impaired (*3*). This is especially problematic when the POI has a short half-life. Here, we establish a new positive selection screening method to identify protein degraders. Using this method, we performed an arrayed small-molecule screen to identify novel degraders of IKZF1, as well as a pooled genetic screen to identify cyclin-dependent kinase 2 (CDK2) as a regulator of the neuroendocrine transcription factor Achaete-scute homolog 1 (ASCL1).

RESULTS AND DISCUSSION

To develop a positive selection assay for protein degraders, we made a bicistronic lentivirus encoding (i) a POI fused to a modified version of deoxycytidine kinase (hereafter called DCK*) that converts the non-natural nucleoside 2-bromovinyldeoxyuridine (BVdU) into a poison (*4*) and (ii) green fluorescent protein (GFP). We reasoned that GFP could be used to mark reporter-positive cells, to FACS (fluorescence-activated cell sorting) sort for cells with the desired reporter mRNA levels, and to count cells in multiwell plate assays. In our initial proof-of-concept experiments, we used this virus to create 293FT cells expressing the IMiD target IKZF1 (*1*, *2*, *5*) fused to DCK* and compared them to cells expressing unfused DCK* or unfused IKZF1 (Fig. 1, A and B). As expected, the IMiD pomalidomide (POM) down-regulated DCK*-IKFZ1 and IKZF1 but not DCK* (Fig. 1B). We also confirmed that 293FT cells expressing DCK*-IKZF1 or unfused DCK* were more sensitive to BVdU than 293FT cells expressing IKZF1 alone or infected with an empty vector (EV) (Fig. 1C). The increased BVdU sensitivity of the DCK* cells relative to the DCK*-IKZF1 cells is likely explained by the higher protein levels of

[1]Department of Medical Oncology, Dana-Farber Cancer Institute, Boston, MA 02215, USA. [2]Department of Cancer Biology, Dana-Farber Cancer Institute, Boston, MA 02215, USA. [3]Department of Biological Chemistry and Molecular Pharmacology, Harvard Medical School, Boston, MA 02115, USA. [4]Ludwig Cancer Center, Boston, MA 02115, USA. [5]Department of Cell Biology, Harvard Medical School, Boston, MA 02115, USA. [6]Linde Program in Chemical Biology, Dana-Farber Cancer Institute, Boston, MA 02215, USA. [7]Broad Institute of MIT and Harvard, Cambridge, MA 02142, USA. [8]Novartis Institutes for Biomedical Research, Cambridge, MA 02139, USA. [9]Departments of Pediatrics and Biochemistry, Medical College of Wisconsin, Milwaukee, WI 53226, USA. [10]Lowe Center for Thoracic Oncology, Dana-Farber Cancer Institute, Boston, MA 02215, USA. [11]Department of Medicine, Brigham and Women's Hospital, Harvard Medical School, Boston, MA 02215, USA. [12]Howard Hughes Medical Institute, Chevy Chase, MD 20815, USA.
*These authors contributed equally to this work.
†Present address: Novartis Institutes for Biomedical Research, Cambridge, MA 02139, USA.
‡Present address: Department of Biomedical Genetics and Wilmot Cancer Institute University of Rochester Medical Center, 601 Elmwood Ave, Rochester, NY 14642, USA.
§Present address: Meyer Cancer Center and The Biochemistry, Structural, Developmental, Cell and Molecular Biology Allied PhD Program, Weill Cornell Medicine, New York, NY 10021, USA.
‖Present address: Tango Therapeutics, Cambridge, MA 02142, USA.
¶Corresponding author. Email: moser@partners.org (M.G.O.); william_kaelin@dfci.harvard.edu (W.G.K.)

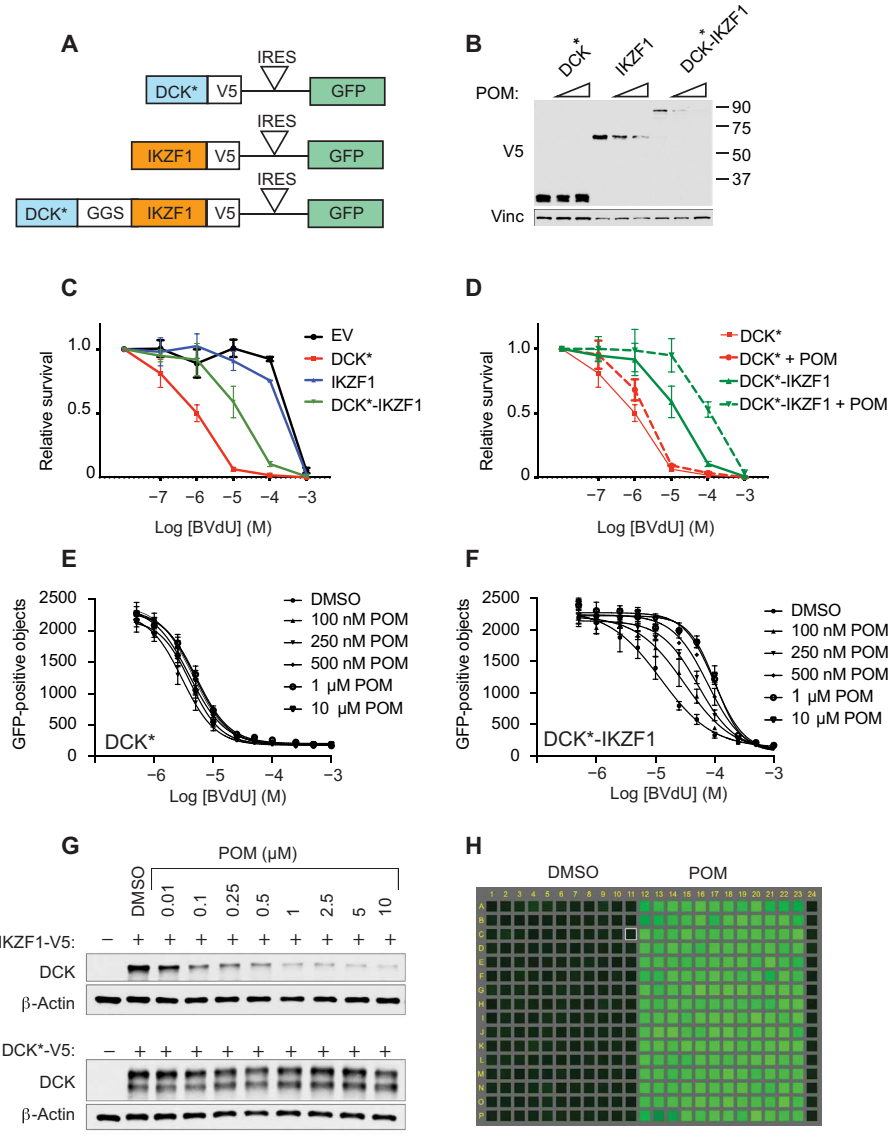

Fig. 1. Design of positive selection assay for protein degraders. (**A**) Vector schematic. DCK*, variant deoxycytidine kinase with Ser74Glu, Arg104Met, and Asp133Ala substitutions; V5, V5 epitope tag; GGS, Gly-Gly-Ser spacer; IRES, internal ribosomal entry site. (**B**) Immunoblot analysis of 293FT cells infected with the lentiviral vectors depicted in (A) and then treated with 1 or 10 μM POM, as indicated by the triangles, for 24 hours. (**C** and **D**) Relative survival of 293FT cells infected with the lentiviral vectors depicted in (A) and then treated with the indicated concentrations of BVdU for 4 days. In (D), cells were also treated with 1 μM (POM) starting 24 hours before BVdU was added. $n = 3$ biological replicates. (**E** and **F**) Number of GFP-positive 293FT cells infected to produce DCK* (E) or DCK*-IKZF1 (F) using the vectors in depicted in (A) and then treated with indicated concentrations of POM and BVdU in 384-well plate format. POM was added 24 hours before treatment with BVdU for 4 days. $n = 4$ biological replicates. (**G**) Immunoblot analyses of cells treated as in (E) and (F). (**H**) Fluorescence data of 384-well plate containing 293FT cells expressing DCK*-IKZF1 treated with DMSO (columns 1 to 11 and 24) or 1 μM POM (columns 12 to 23), followed 24 hours later by the addition of 100 μM BVdU for 4 days (columns 1 to 24).

DCK* compared to DCK*-IKZF1 (Fig. 1B). Similar results were observed with cells expressing DCK*-K-Ras (G12V), DCK*-Cyclin D1, DCK*-FOXP3, and DCK*-MYC, indicating that DCK* remains active when fused to a variety of proteins (fig. S1). POM increased the BVdU median effective concentration (EC_{50}) of cells expressing DCK*-IKZF1 but not of cells expressing DCK* (Fig. 1D).

Next, we seeded either the DCK*-IKZF1 cells or DCK* cells in 384-well plates and treated the wells with increasing amounts of POM or with dimethyl sulfoxide (DMSO). We added BVdU 24 hours later and measured cell viability 4 days thereafter by measuring the number of GFP-positive objects per well. POM again promoted the survival of the DCK*-IKZF1 cells, but not the DCK* cells, over a range of POM and BVdU concentrations (Fig. 1, E to G). In anticipation of using this assay for a high-throughput screen, we next seeded the DCK*-IKZF1 cells in 384-well plates and treated half the wells with POM and half the wells with DMSO, followed 24 hours later by BVdU (Fig. 1H). Measuring GFP-positive objects 4 days later produced a favorable Z' value (0.7) for this assay.

Encouraged by these findings, we did a pilot screen with 293FT cells expressing DCK*-IKZF1 or unfused DCK* grown in 384-well plates and a library of ~2000 bioactive compounds, which included lenalidomide (LEN) and POM (Fig. 2, A to C). Each well received a

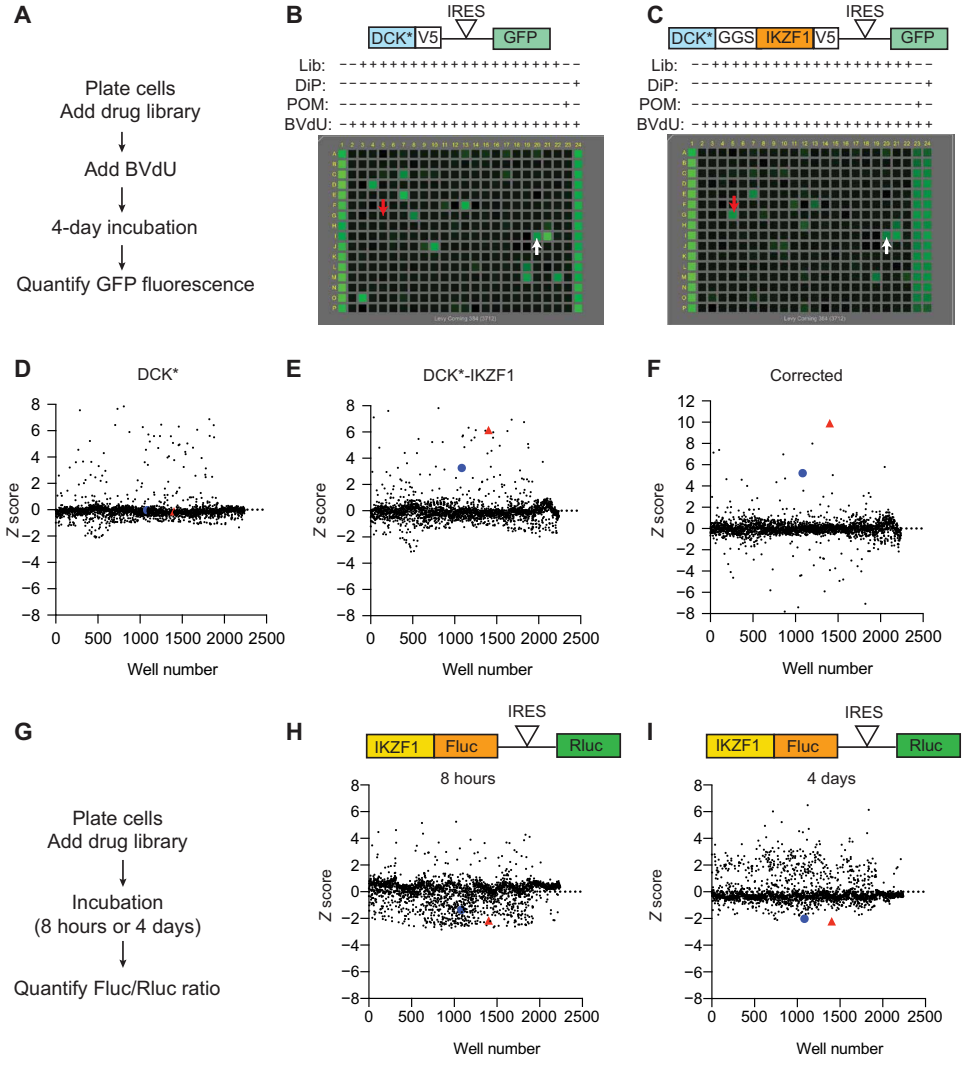

Fig. 2. Comparison of positive selection and negative selection protein degradation assays. (**A**) Scheme for positive selection protein degradation assay. (**B** and **C**) Representative fluorescence data of 384-well plates containing 293FT cells expressing DCK* (B) or DCK*-IKZF1 (C) treated with compounds in the Selleck BioActive Library (one compound per well), followed 24 hours later by the addition of BVdU at the EC_{85} (10 and 100 μM, respectively) for 4 days. BVdU was omitted in column 1. Columns 23 and 24 contained 10 μM POM and 12.5 μM dipyridamole (DiP), respectively. Library wells containing POM and DiP are indicated by the red and white arrows, respectively. (**D** and **E**) Z-distribution of GFP fluorescence of DCK* cells (D) and DCK*-IKZF1 cells (E) screened with the full Selleck BioActive Library. LEN and POM are indicted by the blue circle and red triangle, respectively. $n = 2$ biological replicates. (**F**) Corrected *z* scores obtained by subtracting *z* scores in (D) from *z* scores in (E). (**G**) Scheme for negative selection screening using the dual-luciferase reporter assay. (**H** and **I**) *Z* scores of Fluc/Rluc ratio of 293FT IKZF1-Fluc-IRES-Rluc cells after screening with the Selleck BioActive Library for 8 hours (H) or 4 days (I). $n = 2$ biological replicates.

different compound at a concentration of approximately 10 μM by pin transfer, followed the next day by BVdU. BVdU was added at 100 μM to the DCK*-IKZF1 cells and at 10 μM to the DCK* cells to achieve comparable cell killing despite the higher levels of DCK* relative to DCK*-IKZF1 (fig. S2). Four days thereafter, the GFP fluorescence for each well was measured and converted to a *z* score based on the GFP fluorescence values for the other wells on its plate. LEN and POM scored positively ($z > 2$) in the DCK*-IKZF1 screen but not the DCK* screen (Fig. 2, B to E). Some compounds promoted the survival of both DCK* cells and the DCK*-IKZF1 cells, including compounds that interfere with BVdU uptake (e.g., dipyridamole) (*6*, *7*) or incorporation into DNA (e.g., thymidine) (compare Fig. 2, B and C). Such assay positives could be largely eliminated by subtracting the DCK* *z* score for each chemical from its DCK*-IKZF1 *z* score (Fig. 2F). For comparative purposes, we also did a screen with the same 2000 bioactive compound collection using 293FT cells expressing a bicistronic mRNA encoding (i) an IKZF1–Firefly luciferase (Fluc) fusion and (ii) Renilla luciferase (Rluc), using a decrease in the Fluc/Rluc ratio to identify IKZF1 degraders (Fig. 2, G to I, and fig. S3) (*2*). As expected for such a down assay, this screen underperformed the DCK*-IKZF1 up screen with respect to both signal to noise and the number of false positives, which included compounds that inhibit Cap-dependent translation (e.g., VX-11e or BIX02565) (*8*–*10*). Compounds that nonselectively inhibit transcription, translation, or protein folding would predictably be especially problematic for Fluc fusions with shorter half-lives than the Rluc internal control. Notably, the

transcriptional inhibitor actinomycin D and the translational inhibitor cycloheximide did not promote the survival of the DCK*-IKZF1 cells at any concentration tested (fig. S4).

As one way to minimize false positives, we seeded 384-well plates with a 1:1 mixture of 293FT cells expressing either (i) DCK*-IKZF1 and GFP or (ii) DCK* and TdTomato (Fig. 3A). Both POM and dipyridamole increased the number of GFP-positive cells, but dipyridamole was readily identified as a false positive by examining the TdTomato fluorescence channel (Fig. 3B). We then repeated these experiments in 384-well plate format, exposing the cells to 10 different concentrations of a small library of approximately 100 analogs of POM that we had synthesized, which included the known IKZF1 degraders LEN, POM, and avadomide (MI-2-65) (*11*) and several uncharacterized IMiD-like molecules from the literature (*12*) (Fig. 3C and tables S1 and S2). This library was generated to test whether our assay could correctly identify the known IKZF1 degraders and identify additional IKZF1 degraders made by alternative diversification of the aryl moiety of POM. LEN, POM, and avadomide all scored in our assay (Fig. 3C). In addition, several previously uncharacterized compounds, including MI-2-61 and MI-2-197, appeared to be at least as potent as POM in this screen and in confirmatory immunoblot assays (Fig. 3, C to F, and fig. S5). Our screen also correctly classified compounds that did not down-regulate IKZF1 in immunoblot assays, including some (e.g., MI-2-192 and MI-2-118) that still bound to cereblon in biochemical assays (fig. S5).

To begin looking for non-IMiD IKZF1 degraders, we screened ~546 metabolic inhibitors and anticancer drugs at 10 different concentrations using the DCK*-IKZF1 293FT cells in 384-well plate format (tables S3 and S4) (*13*). In parallel, we counterscreened against unfused DCK* cells. Spautin-1 (*14*), like POM, promoted the survival of the DCK*-IKZF1 cells, but not the DCK* cells, in a dose-dependent manner (Fig. 4, A to D). We confirmed that Spautin-1 down-regulated DCK*-IKZF1 and V5-tagged exogenous IKZF1 but not DCK* (Fig. 4E). IKZF1-V5 was among the 100 most down-regulated proteins after 24 hours of Spautin-1 treatment, as determined by quantitative mass spectrometry proteomics (fig. S6 and table S5). Until the direct target of Spautin-1 linked to IKZF1 turnover is known, it is impossible to know how many of these changes in protein abundance are direct versus indirect and on-target versus off-target. Notably, Spautin-1, unlike POM, down-regulated IKZF1 in cells lacking cereblon (Fig. 4F).

Spautin-1 reportedly suppresses autophagy by inhibiting the USP10 and USP13 deubiquitinases (*14*). IKZF1 protein levels were not decreased after small interfering RNA–mediated down-regulation of USP10, alone or in combination with USP13 (fig. S7A), and Spautin-1's ability to down-regulate IKZF1 was not altered when one or both of these proteins were suppressed (fig. S7, B and C). Moreover, Spautin-1 down-regulated IKZF1 in 293FT cells in which autophagy was disabled by CRISPR-Cas9–mediated disruption of ATG7, Beclin1, or FIP200 (fig. S8).

In contrast, down-regulation of IKZF1 by Spautin-1 was blocked by compounds that inhibit either the E1 ubiquitin activating enzyme or the proteasome (Fig. 4G). Down-regulation of IKZF1 by Spautin-1 was not, however, blocked by an inhibitor of neddylation, which is required for cullin-dependent ubiquitin ligases [e.g., the cereblon-containing ubiquitin E3 ligase that is coopted by the IMiDs (*1*, *2*, *5*)] (Fig. 4G). Down-regulation of exogenous IKZF1 by Spautin-1 requires the IKZF1 N-terminal region containing IKZF1's first zinc finger domain (ZF1) but not the IKZF1 zinc finger domain (ZF2) targeted by the IMiDs (fig. S9, A and B) (*15*, *16*). The down-regulation of the N terminus of IKZF1 was similarly blocked by compounds that inhibit either the E1 ubiquitin activating enzyme or the proteasome but not by inhibitors of neddylation (fig. S9C). Preliminary structure-activity relationship studies identified both active and inactive Spautin-1 derivatives (fig. S10), suggesting that down-regulation of IKZF1 by Spautin-1 reflects a specific protein-binding event and that Spautin-1's potency and specificity can be optimized further.

The experiments described above implied that Spautin-1 post-transcriptionally regulates IKZF1. Nonetheless, Spautin-1 also suppressed exogenous IKZF1 mRNA levels in 293FT cells (fig. S11). However, Spautin-1 suppressed endogenous IKZF1 protein levels in KMS11 and L363 myeloma cells at concentrations that minimally suppressed IKZF1 mRNA levels (Fig. 4, H and I, and fig. S12, A to C). Spautin-1 did not down-regulate IKZF1 in all myeloma cells tested (fig. S12, D and E). The biochemical basis for this variability is not clear.

Notably, down-regulation of IKZF1 by Spautin-1 occurs much more slowly than with IMiDs, suggesting that its effect on IKZF1 is indirect (fig. S13). Nonetheless, its ability to score in a positive selection assay, as well as its inability to down-regulate IKZF1 in some myeloma lines, suggests that it is not broadly toxic at concentrations that down-regulate IKZF1. We are currently seeking the direct Spautin-1 target linked to IKZF1 turnover using genetic and biochemical tools.

One advantage of positive selection assays is their enablement of pooled screens. Our positive selection assay, however, uses a suicide gene. Some suicide genes cause bystander killing that could confound their use in pooled screens. In pilot studies, however, we confirmed that DCK*-IKZF1 cells rapidly outgrew DCK* cells in cocultures treated with IMiDs and BVdU (fig. S14A) and that the DCK* single guide RNA (sgRNA) was rapidly and specifically enriched relative to the control sgRNA in Cas9-positive 293FT cells expressing either DCK*-IKZF1 or DCK*-FOXP3 and then treated with BVdU (fig. S14, B and C). Therefore, bystander killing is negligible in this system.

To begin to address the general utility of our methodology, as well as its ability to function in a pooled format, we next did experiments with ASCL1 in place of IKZF1. ASCL1 is an undruggable lineage-specific transcription factor that is required for survival in many small cell lung cancers (SCLCs) and neuroblastomas (*17*–*19*). We made Jurkat T cells that express Cas9 and either (i) DCK*, (ii) the neural/neuroendocrine lineage–specific transcription factor ASCL1, (iii) DCK*-ASCL1, or (iv) ASCL1-DCK* (Fig. 5A and fig. S15A). Jurkat cells were chosen because they are easily grown and expanded in suspension cultures. ASCL1-DCK* was chosen for further study because we could not generate cells producing high levels of DCK*-ASCL1 (fig. S15A). We first confirmed that ASCL1-DCK* expression sensitized Jurkat cells to BVdU and that this was partially reversed after down-regulating the fusion with ASCL1 sgRNAs (Fig. 5, A and B, and fig. S16, A and B). Cas9 expression was also slightly attenuated in the ASCL1-DCK* cells over time for unclear reasons (Fig. 5A). Nonetheless, these cells efficiently edited a GFP-based reporter of Cas9 activity within 10 days of receiving a GFP sgRNA (fig. S15, B and C). Next, we infected the ASCL1-DCK* and DCK* cells with a lentiviral sgRNA library targeting 788 genes (seven sgRNAs per gene) that encode druggable proteins (table S6). Ten days later (to allow time for gene editing), the cells were split and grown in the presence of 200 or 500 μM BVdU for an

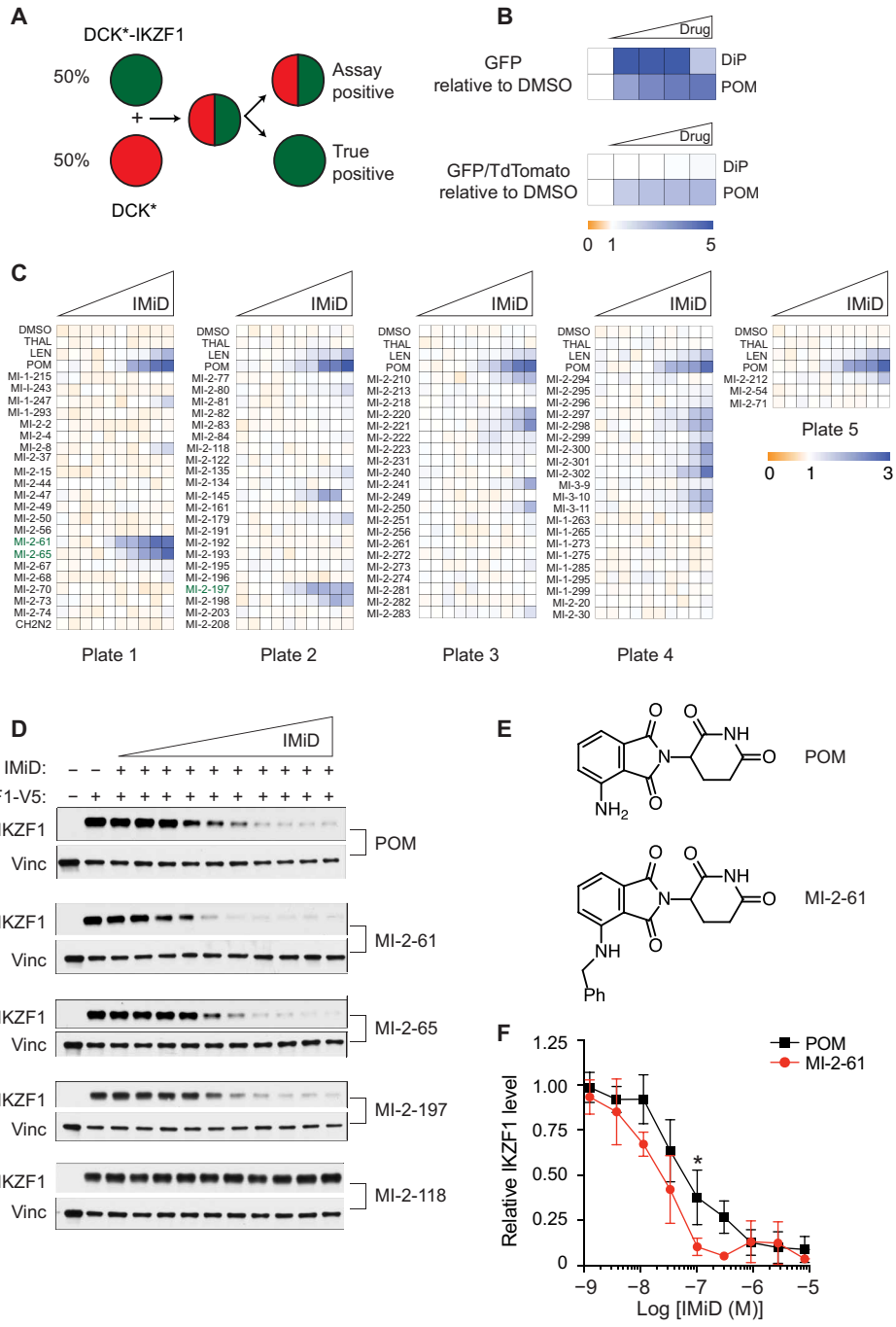

Fig. 3. Identification of novel IMiDs using multiplexed positive selection protein degradation assay. (**A**) Scheme for in-well GFP/TdTomato competition assay. 293FT cells were infected to produce DCK*-IKZF1 and GFP or DCK* and TdTomato using bicistronic vectors analogous to those depicted in Fig. 1A. (**B**) Top: Heatmap of the fold change (relative to treatment with DMSO) of GFP fluorescence of a 1:1 mixture of GFP-positive DCK*-IKZF1 and TdTomato-positive DCK* cells treated with 3.125, 6.25, 12.5, or 25 μM POM or dipyridamole or with vehicle (DMSO) and followed 1 day later by the addition of 100 μM BVdU for 4 days. Bottom: Heatmap of the fold change (relative to treatment with DMSO) of the ratio of GFP fluorescence to TdTomato fluorescence of the cells treated in (A). $n = 2$ biological replicates. (**C**) Heatmap of the fold change (relative to treatment with DMSO) of the ratio of GFP to TdTomato fluorescence of a 1:1 mixture of GFP-positive DCK*-IKZF1 and TdTomato-positive DCK* cells treated with 1.3 nM, 3.8 nM, 11.4 nM, 34 nM, 102 nM, 310 nM, 920 nM, 2.78 μM, 8.33 μM, and 25 μM of the indicated IMiDs, as indicated by the triangles, or with vehicle (DMSO), and followed 1 day later by the addition of 100 μM BVdU for 4 days. $n = 2$ biological replicates. (**D**) Immunoblot analysis of 293FT cells lentivirally transduced to express IKZF1-V5 and treated with the indicated IMiD derivatives for 24 hours using the same concentration range as in (C). (**E**) Structures of POM and IMiD MI-2-61. (**F**) Quantification of immunoblot data in (D); $n = 2$ biological replicates.

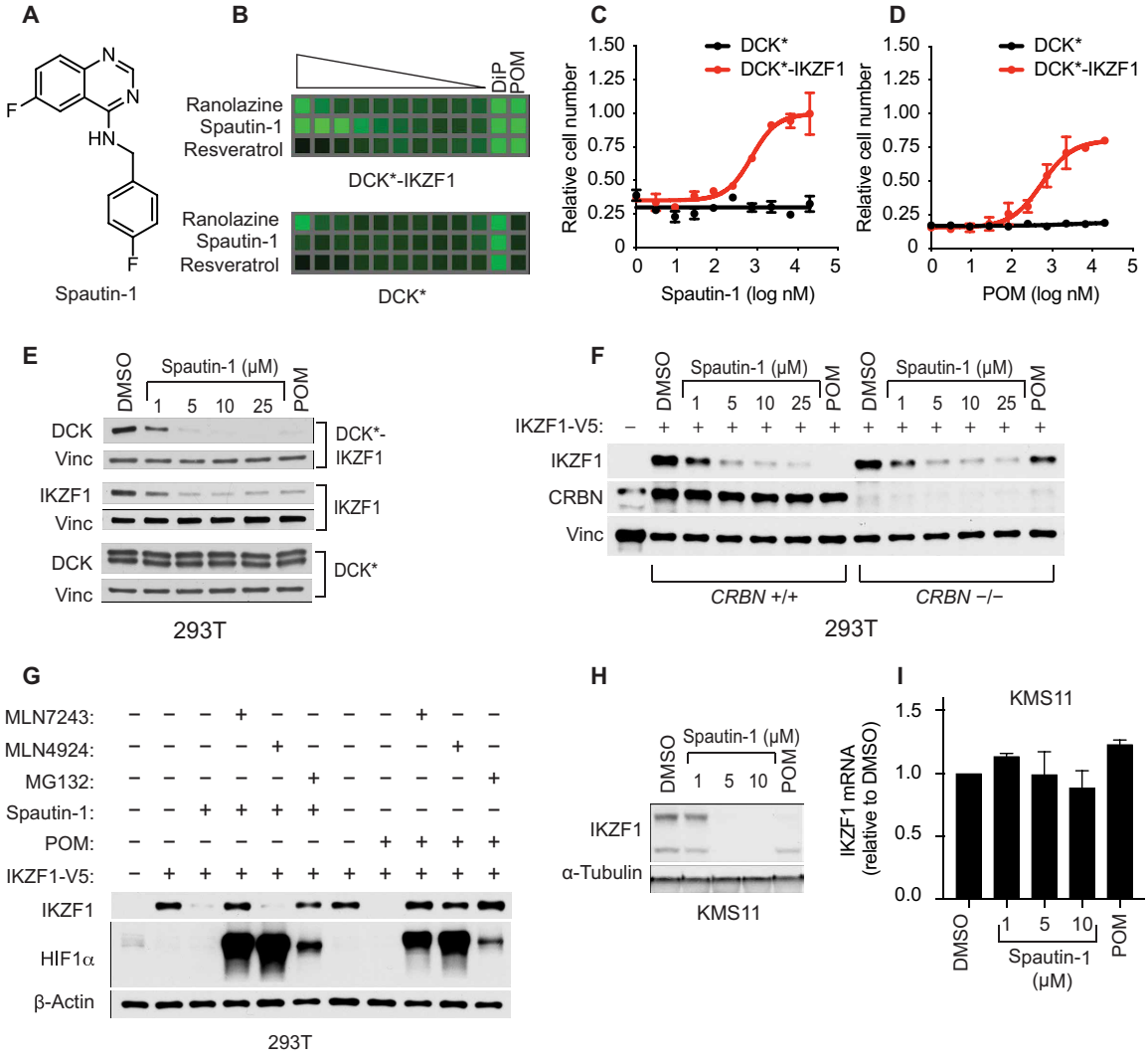

Fig. 4. Spautin-1 targets IKZF1 for proteasomal degradation in a cereblon-independent manner. (**A**) Chemical structure of Spautin-1. (**B**) GFP fluorescence of DCK*-IKZF1 and DCK* 293FT cells treated with ranolazine, Spautin-1, and resveratrol at concentrations of 25 μM, 8.33 μM, 2.78 μM, 920 nM, 310 nM, 102 nM, 34 nM, 11.4 nM, 3.8 nM, and 1.3 nM, as indicated by the triangle, followed 24 hours later by the addition of BVdU at the EC_{85}. Shown for comparison are cells treated with POM (10 μM) or dipyridamole (DiP) (12.5 μM) before adding BVdU. $n = 2$ biological replicates. (**C** and **D**) Quantification of GFP fluorescence from (B) for Spautin-1 (C) and for an analogous titration with POM (D). (**E**) Immunoblot analysis of 293FT cells infected with lentiviruses as in Fig. 1A and treated with the indicated concentrations of Spautin-1 for 24 hours. (**F**) Immunoblot analysis of isogenic 293FT *CRBN* $^{+/+}$ and *CRBN* $^{-/-}$ cells transduced to express IKZF1-V5 and treated with the indicated concentrations of Spautin-1 or POM (1 μM) for 24 hours. (**G**) Immunoblot analysis of 293FT cells stably expressing IKZF1-V5 and simultaneously treated with MLN7243 (1 μM), MLN4924 (1 μM), MG132 (1 μM), Spautin-1 (10 μM), or POM (1 μM) for 24 hours as indicated. (**H** and **I**) Immunoblot (H) and RT-qPCR (I) analysis of KMS11 multiple myeloma cells treated with indicated concentrations of Spautin-1 or POM (1 μM) for 24 hours. $n = 3$ biological replicates.

additional 2 weeks (fig. S16C). We then determined sgRNA abundance by next-generation sequencing of genomic DNA and analyzed relative enrichment of sgRNAs compared to the time point before BVdU treatment (fig. S16D). We identified multiple sgRNAs against *CDK2* that were markedly enriched at both BVdU concentrations in the ASCL1-DCK* cells but not the DCK* cells (Fig. 5C, fig. S16, D and E, and table S7).

In validation studies, ASCL1-DCK* Jurkat cells expressing *CDK2* sgRNAs outcompeted ASCL1-DCK* cells expressing control sgRNAs in the presence of BVdU but not in the presence of DMSO (Fig. 5D and fig. S16F). *CDK2* sgRNAs also posttranscriptionally down-regulated ASCL1-DCK* protein levels in the Jurkat cells (Fig. 5, E and F) and endogenous, unfused, ASCL1 in human SCLC lines (NCI-H1876 and NCI-H2081) (Fig. 6, A and B, and fig. S18, A and B). Down-regulation of exogenous ASCL1 in Jurkat cells treated with a CDK2 sgRNA was rescued by an sgRNA-resistant CDK2 complementary DNA (cDNA) encoding wild-type CDK2 but not kinase-dead CDK2 (Fig. 5G). The kinase-dead CDK2 was, however, produced at slightly lower levels, presumably because it is less stable or because of its known dominant-negative effects due to cyclin sequestration (*20*–*22*).

CDK2 has been well recognized as a potential anticancer target. The development of selective small-molecule CDK2 inhibitors, however, has been hampered by their off-target effects on other CDK family members, especially the broadly essential kinase CDK1. We verified that well-established CDK2 inhibitor dinaciclib (*23*) down-regulated both ASCL1 protein and mRNA levels (fig. S17, A to D),

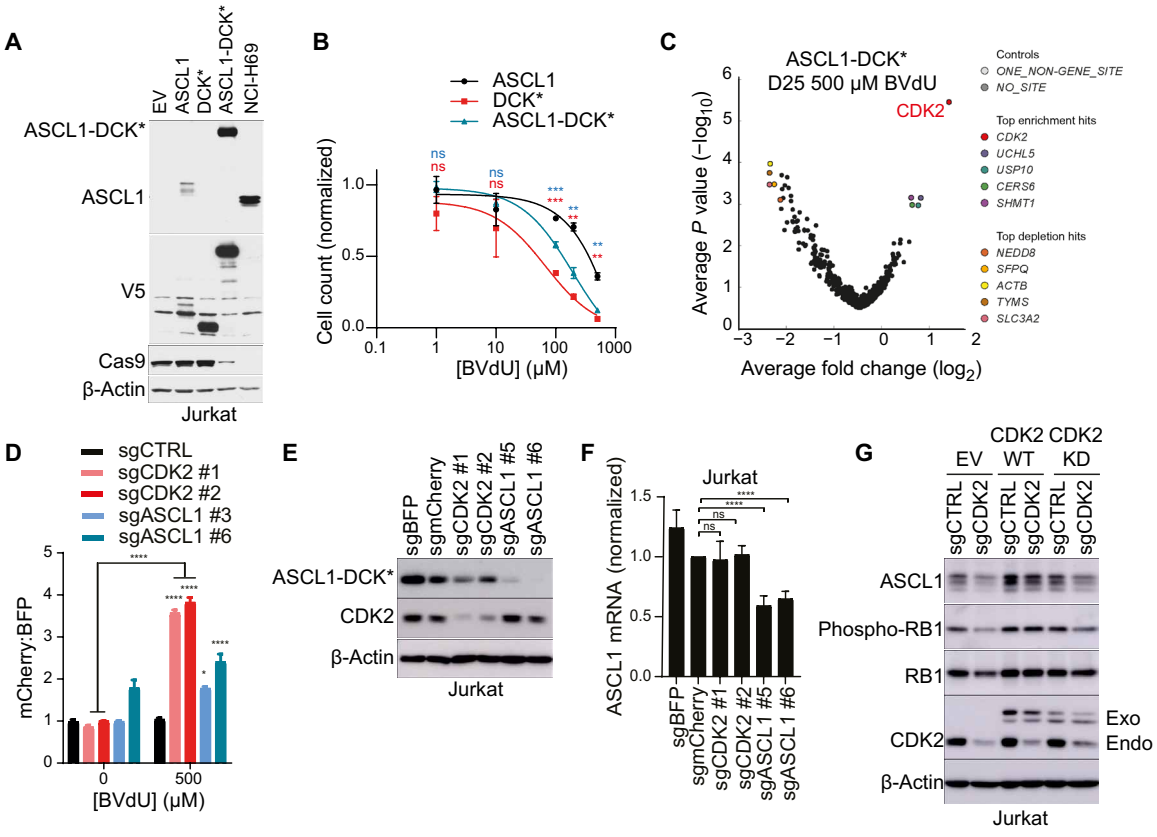

Fig. 5. Identification of CDK2 as an ASCL1 protein stabilizer using CRISPR-Cas9 positive selection screening. (**A**) Immunoblot analysis of Jurkat cells first infected to express Cas9 and then superinfected to express exogenous ASCL1, DCK*, or the ASCL1-DCK* fusion. NCI-H69 cells are included as a benchmark for ASCL1 endogenous expression. (**B**) Growth inhibition (%), based on viable cell numbers relative to untreated controls, of the indicated cell lines from (A) treated with BVdU for 6 days. $n = 2$ biological replicates. (**C**) Hypergeometric analysis of BVdU positive selection CRISPR-Cas9 screen on day 25 relative to day 10 (early time point before BVdU treatment) of ASCL1-DCK* Cas9 Jurkat cells treated with 500 μM BVdU. $n = 2$ biological replicates. (**D**) Quantification of fold change in mCherry:BFP ratio after 18 days of 500 μM BVdU or DMSO (0) treatment of ASCL1-DCK* Cas9 Jurkat cells expressing the indicated sgRNAs and mCherry or a nontargeting control sgRNA and blue fluorescent protein (BFP) (initially mixed 1:3). $n = 3$ biological replicates. (**E**) Immunoblot and (**F**) RT-qPCR analysis of ASCL1-DCK* Cas9 Jurkat cells superinfected to express the indicated sgRNAs. $n = 4$ biological replicates. (**G**) Immunoblot analysis of Jurkat cells first infected with a lentivirus to stably express exogenous ASCL1, then infected with Dox-inducible (DOX-On) sgRNA-resistant CDK2 wild-type (WT) or CDK2 kinase-dead (KD) mutant, and lastly superinfected with a CDK2 or nontargeting sgRNA. Following superinfection with the sgRNA lentiviruses, cells were grown in DOX to maintain exogenous CDK2 expression. $n = 4$ biological replicates. Exo, exogenous CDK2; Endo, endogenous CDK2. Error bars represent SD. ns, nonsignificant; *$P < 0.05$; ***$P < 0.001$; ****$P < 0.0001$.

potentially due to its polypharmacological activity on both CDK2 and other CDKs such as CDK9 (*23*, *24*). We obtained, however, two small-molecule CDK2 degraders (TMX-2138 and TMX-2172) that more selectively target CDK2 through recruitment of cereblon (*25*). Both of these compounds down-regulated ASCL1 protein levels in both human (NCI-H1876 and NCI-H1092) and mouse (97-2 and 188) SCLC lines (Fig. 6, C to F, and fig. S18, C to F). For unclear reasons, ASCL1 was down-regulated more rapidly in the mouse lines than in the human lines. We focused on TMX-2172 because TMX-2138 also suppressed *ASCL1* mRNA levels in the mouse cells (Fig. 6F and fig. S18F). TMX-2172 decreased the half-life of ASCL1 protein (Fig. 6, G and H), consistent with posttranscriptional regulation of ASCL1 by CDK2.

We conducted our screens in IKZF1-independent 293FT cells rather than IKZF1-dependent myeloma cells and in ASCL1-independent Jurkat cells rather than in ASCL1-dependent SCLC cells in an attempt to preserve positive selection. It is possible, however, that some degradation mechanisms will be highly context dependent and restricted to the therapeutic target cell of interest. We also anticipate that some DCK* fusion proteins will not be functional due to steric or conformational effects. This might be remedied by fusing DCK* to the alternative POI terminus (N-terminus versus C-terminus), by exploring different linkers, or using alternative suicide proteins.

IMiDs are important multiple myeloma drugs, but loss of cereblon has emerged as an important mechanism of IMiD resistance (*26*–*28*). Identification of Spautin-1's mechanism of action could eventually lead to drugs for circumventing this problem.

ASCL1 is a sequence-specific DNA binding transcription factor that would classically be deemed undruggable and serves as a lineage addiction oncoprotein in neural crest–derived tumors, such as SCLCs and neuroblastomas (*17*–*19*, *29*). Genetic studies in *Xenopus* indicate that CDK2 regulates ASCL1 function and that ASCL1 contains multiple potential CDK2 phosphorylation sites that prevent it from inducing neuronal differentiation (*30*, *31*). CDK2 is a potential dependency in some neuroblastomas (*32*–*34*). CDK2 and N-MYC drive the accumulation of phosphorylated ASCL1 in undifferentiated

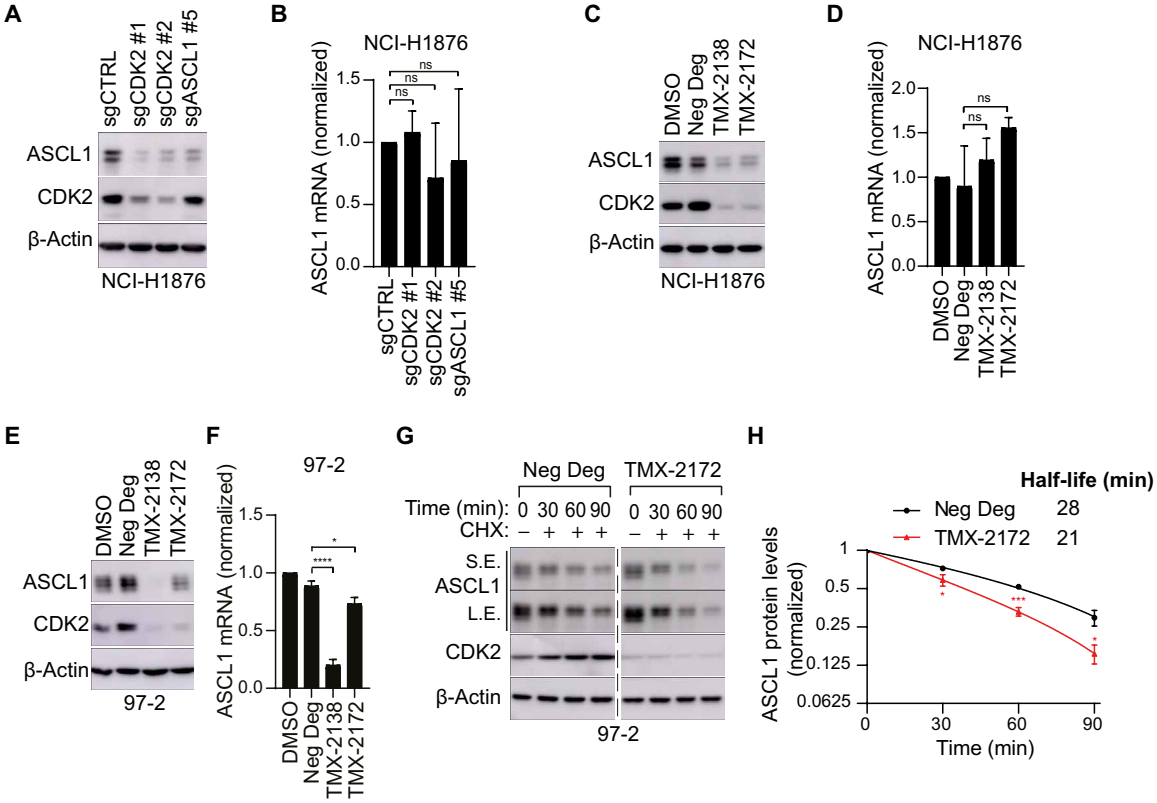

Fig. 6. CDK2 inactivation destabilizes ASCL1 protein in SCLC cell lines. (**A**) Immunoblot and (**B**) RT-qPCR analysis of the NCI-H1876 SCLC cell line that endogenously expresses ASCL1 infected to express the indicated sgRNAs. $n = 3$ biological replicates. (**C** and **E**) Immunoblot and (**D** and **F**) RT-qPCR analysis of NCI-H1876 human SCLC cells (C and D) and 97-2 mouse SCLC cells (E and F) after treatment with the CDK2 PROTAC degraders (TMX-2138 and TMX-2172) or the indicated negative controls, all used at 500 nM for either 36 hours (C and D) or 8 hours (E and F). Neg Deg, negative control degrader ZXH-7035. $n = 3$ biological replicates. (**G**) Immunoblot analysis and (**H**) quantification of ASCL1 protein levels in 97-2 cells first treated with the CDK2 PROTAC degrader or negative control (500 nM) for 4 hours and then treated with cycloheximide (CHX) (150 μg/ml) for the indicated times. S.E., short exposure; L.E., long exposure. $n = 4$ biological replicates. In all experiments, error bars represent SD except in (H), where error bars represent SEM. *$P < 0.05$; ***$P < 0.001$; ****$P < 0.0001$.

neuroblastomas (*31*). Conversely, loss of CDK2 activity, such as through retinoic acid–mediated induction of p27 or small-molecule inhibitors, is associated with neuroblastoma differentiation and decreased tumor formation (*32*–*37*). It will be important to determine how, mechanistically, CDK2 regulates ASCL1 turnover. In particular, we have not yet shown that the regulation of ASCL1 by CDK2 is direct. Nonetheless, our study provides further support for CDK2 as a potential therapeutic target in SCLC and neuroblastoma.

The discovery that the IMiDs reprogram the cereblon ubiquitin E3 ligase for therapeutic benefit has galvanized interest in identifying compounds that can degrade, directly and indirectly, otherwise undruggable proteins. Sometimes, one can engineer heterobifunctional degrader molecules consisting of a POI-binding moiety, a linker, and a ubiquitin-ligase recruitment moiety (*38*). This approach requires a ligand with suitable binding affinity for the POI, and identifying a successful linker often requires multiple iterations of trial and error. Moreover, this approach fails to harness the many other ways a chemical could directly or indirectly degrade a protein, such as by inhibiting a deubiquitinating enzyme, displacing an interacting protein, or altering protein folding or subcellular localization. A trivial way to down-regulate proteins, especially those with naturally rapid turnovers, is to poison transcription or translation. The screening methodology described here should facilitate the characterization of designer degraders as well as enable mechanism-agnostic searches for compounds and targets that regulate the abundance of previously undruggable proteins.

METHODS

Cell culture

293FT cells were originally obtained from the American Type Culture Collection (ATCC). 293AD cells were from Cell Biolabs. 293FT *CRBN*$^{-/-}$ cells were made by CRISPR-Cas9 editing (see below). 293FT and 293AD cells were maintained in Dulbecco's minimum essential medium (DMEM) supplemented with 10% fetal bovine serum (FBS), penicillin (100 U/ml), and streptomycin (100 μg/ml). KMS11, KMS34, MM.1S, and L363 human multiple myeloma cells [gift of K. Anderson (Dana-Farber Cancer Institute)] and Jurkat cells (obtained from ATCC in September 2016) were maintained in RPMI medium supplemented with 10% FBS, penicillin (100 U/ml), and streptomycin (100 μg/ml). NCI-H1876 (obtained in November 2016), NCI-H1092 (obtained in November 2018), and NCI-H2081 (obtained in November 2018) were obtained from ATCC. NCI-H1876, NCI-H1092, and NCI-H2081 cells were maintained in DMEM/F12 media supplemented with HITES [10 nM hydrocortisone (Sigma-Aldrich, #H0135), insulin (0.01 mg/ml), human transferrin (0.0055 mg/ml),

sodium selenite (0.005 μg/ml) (ITS, Gemini, #400-145), and 10 nM β-estradiol (Sigma-Aldrich, #E2257)] and 5% FBS. The cell lines 188 and 97-2 were isolated from genetically engineered SCLC mouse tumors (see below for description of cell line generation) and maintained in RPMI 1640 media supplemented with HITES and 10% FBS. All cells were grown at 37°C in the presence of 5% CO_2. Fresh aliquots of cells were thawed every 4 to 6 months.

Commercially available compounds

The following compounds were purchased: POM (Selleck, #S1567), LEN (Selleck, #S1029), MG132 (*N*-carbobenzyloxy-L-leucyl-L-leucyl-L-leucinal; Thermo Fisher Scientific, #47479020MG), MLN4924 (Active Biochem, #A-1139), MLN7243 (Thermo Fisher Scientific, #NC1129906), Spautin-1 (BioTechne; #5197/10), cycloheximide (VWR, #97064-724), BVdU (Chem-Impex International Inc., catalog no. 27735), actinomycin D (Thermo Fisher Scientific, #11805017), and dinaciclib (Selleck, #S2768).

CDK2 degraders

Synthesis and characterization of the small-molecule CDK2 degraders TMX-2138 and TMX-2172 and the negative degrader ZXH-7035 (structurally similar to the CDK2 binding region of TMX-2138 and TMX-2172 but lacking the cereblon recruiting element) are described previously (*25*).

FACS sorting for high expression of DCK* fusion proteins

293FT cells stably transduced with bicistronic lentiviruses expressing (i) a fusion between DCK* and the POI and (ii) GFP were seeded at a density of 0.25×10^6 cells/ml in 25 ml of media in a 15-cm dish (Corning, 353025). Two days later, the cells were counted and resuspended in media to a concentration of 10×10^6 cells/ml. The sample was passed through a mesh strainer (Thermo Fisher Scientific, #352235). The GFP fluorescence of the cells was analyzed by FACS using a Fortessa Aria II instrument. The brightest 1% of cells were collected in an Eppendorff tube, replated in a six-well dish, and expanded. This process was repeated three to four more times to isolate cells expressing the desired GFP levels.

Jurkat cells were first transduced with PLL3.7-Cas9-IRES-Neo. Neomycin-resistant cells with confirmed Cas9 expression were then superinfected with pLX304-ASCL1-DCK*-IRES-GFP or pLX304-DCK*-IRES-GFP, and transduced cells were selected with blasticidin. The blasticidin-resistant cells were then prepared for FACS sorting as above. In total, the brightest 1% of cells were FACS-sorted three times to isolate cells expressing the desired GFP levels. Jurkat cells expressing Cas9 and DCK*-FOXP3 were made in an analogous manner.

Immunoblotting

Cell pellets were lysed in a modified EBC lysis buffer [50 mM tris-Cl (pH 8.0), 250 mM NaCl, 0.5% NP-40, and 5 mM EDTA] supplemented with a protease inhibitor cocktail (cOmplete, Roche Applied Science, #11836153001). Whole-cell extracts were quantified using the Bradford protein assay. For experiments with 293FT cells, 10 μg of protein per sample was boiled after adding 3× sample buffer (6.7% SDS, 33% glycerol, 300 mM dithiothreitol, and bromophenol blue) to a final concentration of 1×; resolved by SDS–polyacrylamide gel electrophoresis (PAGE) using either 12.5% SDS-PAGE, Mini-Protean TGX 4 to 15% gels (Bio-Rad, #456-1086), or Criterion TGX gels (Bio-Rad, #5671085); semi-dry transferred onto nitrocellulose membranes; blocked in 5% milk in tris-buffered saline with 0.1% Tween 20 (TBS-T) for 1 hour; and probed with the indicated primary antibodies overnight at 4°C. Membranes were then washed three times in TBS-T, probed with the indicated horseradish peroxidase–conjugated secondary antibodies for 1 hour at room temperature, and washed three times in TBS-T. Bound antibodies were detected with enhanced chemiluminescence Western blotting detection reagents [Immobilon (Thermo Fisher Scientific, #WBKLS0500) or SuperSignal West Pico (Thermo Fisher Scientific, #PI34078)]. The primary antibodies and dilutions used were as follows: rabbit anti-IKZF1 (Cell Signaling Technology, #5443S) at 1:1000, rabbit anti-V5 (Bethyl Laboratories, #A190-120A) at 1:1000, rabbit anti-DCK (Abcam, #151966) at 1:2000, rabbit anti-ASCL1 (Abcam, #ab211327) at 1:1000, rabbit anti-CDK2 (Cell Signaling Technology, #2546S) at 1:1000, mouse anti-P62 (Abcam, #ab56416) at 1:1000, rabbit anti–LC3-I and LC3-II (Cell Signaling Technology, #3868S) at 1:1000, rabbit anti-ATG7L (Cell Signaling Technology, #8558S) at 1:1000, rabbit anti-Beclin1 (Cell Signaling Technology, #3495S) at 1:1000, rabbit anti-FIP200 (Cell Signaling Technology, #12436S) at 1:1000, rabbit α-phospho-RB1 S795 (Cell Signaling Technology, #9301P) at 1:1000, mouse α-RB1 4H1 (Cell Signaling Technology, #9309S) at 1:1000, mouse anti–β-actin (Sigma-Aldrich; clone AC-15, #A3854) at 1:25,000, mouse anti-Cas9 (Cell Signaling Technology, #14697) at 1:1000, mouse anti-vinculin (Sigma-Aldrich; #V9131) at 1:10,000, and mouse anti–β-actin (Cell Signaling Technology, #3700S) at 1:10,000. The secondary antibodies and dilutions used were goat anti-mouse (Pierce) at 1:10,000 and goat anti-rabbit (Pierce) at 1:5000.

Drug treatment of 293FT cells

A total of 750,000 293FT IKZF1-V5 cells per well were seeded in six-well dishes in a volume of 2 ml. On the next day, drugs to be added were diluted from a 10 mM stock (stored at −20°C) into 0.5 ml of media before being added to the cells. The final volume in each well was then made up to 3 ml by adding a second drug in 0.5 ml or adding 0.5 ml of drug-free media.

Drug treatment of multiple myeloma cells

Myeloma cells were seeded in 10-cm plates at a density of 0.75×10^6 cells/ml in a total volume of 8 ml. On the next day, the desired drug was diluted from a 10 mM stock (stored at −20°C) into 1 ml of media, which was added to the intended well to achieve the desired final concentration. The final volume in each well was then made up to 10 ml by adding a second drug in 1 ml or adding 1 ml of drug-free media. After 24 hours, the cells were harvested for analysis.

Low-throughput BVdU treatment curves

293FT cells stably transduced with bicistronic lentiviruses encoding (i) IKZF1, DCK*, or DCK*-IKZF1 (IKZF1 cells, DCK* cells, and DCK*-IKZF1 cells, respectively) and (ii) GFP, as well as corresponding EV control cells, were seeded into six-well plates at 20,000 cells per well in 2.5 ml of media. The next day, 1 M BVdU dissolved in DMSO was diluted into media to prepare 6× stock solutions of BVdU at concentrations of 6 mM, 600 μM, 60 μM, 6 μM, and 600 nM. For each stock solution, DMSO concentration was adjusted to a final concentration of 0.6%. Each well in the six-well dish received 0.5 ml of a 6× stock solution of BVdU to achieve final concentrations of 1 mM, 100 μM, 10 μM, 1 μM, and 100 nM, respectively. A total of 0.5 ml of media with 0.6% DMSO was added to the sixth well as a control. Four days later, the cells were collected and counted using a Vi-Cell XR cell counter.

Low-throughput BVdU treatment curves with POM rescue

293FT cells were seeded as above at a density of 20,000 cells per well in 2 ml of media. A stock solution of 10 mM POM in DMSO was diluted into media to prepare a 6 μM stock solution of POM. Cells received 0.5 ml of the 6 μM POM stock solution to achieve an eventual final concentration of 1 μM or 0.5 ml of control media. The next day, BVdU was added as described above, and cell proliferation was analyzed as above.

Jurkat cells expressing Cas9 and either ASCL1, ASCL1-DCK*, or DCK* alone were plated at 0.05×10^6 cells/ml per well in a 12-well plate and treated with increasing concentrations of BVdU (0, 1, 10, 100, 200, or 500 μM). Six days later, the cells were counted using a Vi-Cell XR cell counter. For ASCL1 sgRNA rescue experiments, Jurkat cells expressing Cas9 and ASCL1-DCK* cells were superinfected with pLentiGuide-Puro–based lentiviruses expressing sgRNAs targeting ASCL1 or a nontargeting sgRNA (sgCTRL). The cells were selected with puromycin, and expression of ASCL1 was analyzed by immunoblot analysis. The cells were then subjected to the BVdU assay as described above.

High-throughput BVdU treatment curves

293FT cells stably transduced with bicistronic lentiviruses encoding (i) DCK*, DCK*-IKZF1, DCK*-K-RAS (G12V), DCK*-Cyclin D1, DCK*-PAX5, DCK*-FOXP3, and DCK*-MYC and (ii) GFP, as well as corresponding EV control cells, were seeded into 384-well plates (Corning, #3764) at 200 cells per well in 30 μl of media. The next day, 1 M BVdU dissolved in DMSO was diluted into media to prepare 4× stock solutions of BVdU at concentrations of 4 mM, 2 mM, 1 mM, 400 μM, 200 μM, 100 μM, 40 μM, 20 μM, 4 μM, and 400 nM. On each plate, 10 μl of each stock concentration of BVdU was added to two columns (32 wells) to achieve final concentrations of 1 mM, 500 μM, 250 μM, 100 μM, 50 μM, 25 μM, 10 μM, 5 μM, 1 μM, and 100 nM. Ten microliters of control media was added to four columns. Four days later, the cells were analyzed using an Acumen laser scanning cytometer (TTP Biosciences). GFP fluorescence was quantified by defining the metric "GFP-positive object" to identify GFP-positive cells while excluding debris or cell fragments.

High-throughput screening using the DCK*-based positive selection assay

Determination of Z′

DCK* and DCK*-IKZF1 cells were seeded into 384-well plates (Corning, #3764) in 30 μl of media at a density of 200 cells per well and allowed to adhere overnight. For each plate, an HPD300 dispenser (Hewlett-Packard) was used to add 4 nl of POM to a final concentration of 1 μM to half the wells. An equal volume of DMSO was added to the other half of the plate. The next day, BVdU was added to the entire plate at a concentration of 10 μM for the plate of DCK* cells and 100 μM for the plate of DCK*-IKZF1 cells. Four days later, the cells were analyzed using an Acumen laser scanning cytometer (TTP Biosciences). The number of GFP-positive objects in each well was measured, and a Z' statistic was calculated comparing the POM-treated wells to the DMSO-treated wells.

High-throughput chemical library screening

DCK* and DCK*-IKZF1 293FT cells were seeded into 384-well plates (Corning, #3764) at a density of 200 cells per well in a volume of 30 μl of media. A custom-built Seiko Compound Transfer Robot was used to pin transfer 100 nl per well of small-molecule stock solutions from the wells of a drug library plate to the wells of assay plate, such that each well of the assay plate received a unique small molecule. An HPD300 non-contact dispenser (Hewlett-Packard) was used to dispense 100 nl of POM and dipyridamole into columns 23 and 24 and to add 100 nl of DMSO to columns 1 and 2. The final concentrations of POM and dipyridamole were 10 μM and 12.5 μM, respectively. The next day, 10 μl of BVdU stock solution was added to columns 2 to 24 of each of the DCK-IKZF1 and DCK* assay plates, respectively. The concentration of the BVdU stock solution was calculated to achieve the desired final concentration of BVdU (10 μM in DCK* assay plates and 100 μM in DCK*-IKZF1 assay plates) in the well.

After 4 days, the GFP fluorescence of each assay plates was quantified using an Acumen scanning laser cytometer. For each plate, the average and SD of the GFP fluorescence of wells in columns 3 to 22 were calculated. For each well on an assay plate, the GFP fluorescence was converted to a z score using the formula: z(well) = [GFP (well) − μ GFP (plate)] / σ GFP (plate), where μ GFP (plate) is the mean GFP fluorescence for that plate and σ GFP (plate) is the SD for that plate.

High-throughput chemical library screening (in-well competition assay)

DCK*-IKZF1 (GFP) and DCK* (Td) cells were mixed together in a 1:1 ratio and then seeded into 384-well plates (Corning, #3764) at a density of 400 cells per well in 30 μl of media. Pin transfer from IMiD derivative library plates and dispensation of POM and dipyridamole were performed as described above. The next day, 10 μl of BVdU stock solution was added to columns 2 to 24 of each plate to achieve a final concentration of 100 μM. After 4 days, the GFP and TdTomato fluorescence of each assay plate was quantified using an Acumen scanning laser cytometer. For each well, the ratio of GFP/tdTomato fluorescence was calculated and normalized to the values in the well that received DMSO and BVdU. The resulting values were converted to a heatmap using Morpheus (Broad Institute).

High-throughput chemical library screening using negative selection assay

Determination of Z′

293FT IKZF1-Fluc cells were seeded into 96-well plates at a density of 2000 cells per well in a volume of 50 μl of media and incubated overnight at 37°C. The next day, an additional 50-μl media and POM (final concentration of 2 μM) was added to 30 wells of the plate (rows B to G, columns 2 to 6). Control media containing DMSO was added to 30 wells of the plate (rows B to G, columns 7 to 11). A Dual-Glo assay (Promega) was performed by first aspirating all media from the tissue culture plates. Twenty-five microliters of a 1:1 dilution of Dual-Glo luciferase assay reagent in phosphate-buffered saline (PBS) was added to wells and incubated for 10 min. Luminescent signal was measured with a plate reader. Stop & Glo reagent (12.5 μl) was then added to the wells, incubated for 10 min, and luminescent signal was measured. The average Fluc/Rluc ratio for cells treated with DMSO and POM was calculated, and a Z' statistic was calculated.

High-throughput library screening using Fluc/Rluc readout

IKZF1-Fluc assay plates were generated by plating 293FT IKZF1-Fluc cells into 384-well plates. For the 8-hour treatment arm, cells were plated at a density of 4000 cells per well. A custom-built Seiko Compound Transfer Robot was used to pin transfer 100 nl per well of small molecule from the drug library plate to the assay plate, such that each well of the assay plates received a unique small molecule. After 8 hours, the plates were shaken out and blotted on clean paper towels to remove the media. A Thermo Multidrop Combi was used

to dispense 20 μl of a 1:1 dilution of Dual-Glo luciferase reagent, and the plates were shaken for 10 min. Firefly luciferase signal was quantified using an EnVision plate reader. A Thermo Multidrop Combi was used to dispense 10 μl of Dual-Glo Stop + Glo reagent, and the plates were shaken for 10 min. Renilla luciferase signal was quantified using an EnVision plate reader. For each plate, the ratios of the Firefly/Renilla luciferase signals were converted to a Z-distribution as outlined above. For the 4-day treatment arm, the experiment was performed in an analogous manner, but the cells were plated at a density of 200 cells per well and were incubated for 4 days before analysis.

sgRNA druggable library construction

Gene-targeting sgRNAs and appropriate controls were designed using the rule set described at the Genetic Perturbation Program (GPP) portal (http://portals.broadinstitute.org/gpp/public). Oligonucleotides were flanked by polymerase chain reaction (PCR) primer sites, and PCR was used to amplify DNA using NEBNext kits. The PCR products were purified using Qiagen PCR cleanup kits and cloned into pXPR_BRD003 using Golden Gate cloning reactions. Pooled libraries were amplified using electrocompetent Stbl4 cells. Viruses were generated as outlined at the GPP portal. The sgRNA library (CP1080, M-AB34) was custom-designed to target cancer-relevant druggable genes. It consisted of 5566 sgRNAs targeting 788 genes (7 sgRNAs targeting each gene) and 300 nontargeting sgRNAs as controls (table S6).

Positive selection CRISPR-Cas9 BVdU resistance screen

Jurkat cells that had been infected with PLL3.7-Cas9-IRES-Neo and subsequently maintained in G418 were then superinfected with pLX304 ASCL1-DCK*-V5-IRES-GFP or pLX304 DCK*-V5-IRES-GFP and placed under blasticidin selection. Blasticidin-resistant cells were sorted for GFP expression (top 1%) three times by FACS. Protein abundance of ASCL1-DCK* or DCK* alone was confirmed by immunoblot analysis, and functionality of ASCL1-DCK* or DCK* alone was determined using BVdU sensitivity and rescue experiments with sgRNAs targeting ASCL1. Cas9 expression was confirmed by immunoblot analysis, and Cas9 activity was confirmed using a Cas9 GFP reporter [pXPR_011 (Addgene, #59702)] (*39*) that showed near maximal editing 10 days after infection.

On day 0, ASCL1-DCK* and DCK* cells expressing Cas9 were expanded and then counted. For each line, 2.2×10^7 cells (~4000 cells per sgRNA) were pelleted and resuspended at 2×10^6 cells/ml in media supplemented with polybrene (8 μg/ml) and infected at a multiplicity of infection (MOI) of ~0.3 with the sgRNA druggable library (CP1080, M-AB34) described above. The cells mixed with polybrene and virus were then plated in 1-ml aliquots onto 12-well plates and centrifuged at 434*g* for 2 hours at 30°C. Sixteen hours later (day 1), the cells were collected, pooled, and centrifuged to remove the virus and polybrene, and the cell pellet was resuspended in complete media at 2×10^5 cells/ml and plated into non–tissue culture–treated t175 flasks. The cells were then cultured for 48 hours before being placed under puromycin (1 μg/ml) drug selection at 4×10^5 cells/ml.

A parallel experiment was performed on day 3 to determine the MOI. To do this, the cells infected with the sgRNA library and mock-infected cells were plated at 4×10^5 cells/ml in the presence or absence of puromycin. After 72 hours (day 6), cells were counted using the Vi-Cell XR cell counter, and the MOI was calculated (which ranged from 0.2 to 0.3 for each replicate) using the following equation: (# of puromycin-resistant cells infected with the sgRNA library / # total cells surviving without puromycin after infection with the sgRNA library) – (# of puromycin-resistant mock-infected cells / # total mock-infected cells).

On day 6 after MOI determination, puromycin-resistant cells were pooled, collected, and counted, and 1×10^8 cells were replated at a concentration of 4×10^5 cells/ml in complete media containing puromycin (1 μg/ml). The remaining cells were discarded. On day 8, again, the puromycin-resistant cells were pooled, collected, and counted, and 1×10^8 cells were replated at a concentration of 4×10^5 cells/ml in complete media containing puromycin (1 μg/ml).

On day 10, puromycin-resistant cells were pooled, collected, and counted. A total of 2×10^7 cells were collected and washed in PBS, and the cell pellets were frozen for genomic DNA isolation for the initial time point before BVdU selection. Then, 2×10^7 cells were resuspended in complete media (now without puromycin) containing either 200 or 500 μM BVdU at a final concentration of 5×10^4 cells/ml and plated into t175-cm flasks. Thus, at least 1000 cells per sgRNA were introduced into BVdU selection.

On day 15, cells treated with 200 or 500 μM BVdU were collected and counted. A total of 10×10^6 cells from each arm of the screen were then resuspended in complete media containing either 200 or 500 μM BVdU at a final concentration of 5×10^4 cells/ml and plated into t175-cm flasks. The remaining cells were centrifuged and washed in PBS, and the cell pellets were frozen. Again, at least 1000 cells per sgRNA were maintained under BVdU selection.

On day 20, cells treated with 200 or 500 μM BVdU were collected and counted. A total of 10×10^6 cells from each arm of the screen were then resuspended in complete media containing either 200 or 500 μM BVdU at a final concentration of 5×10^4 cells/ml and plated into t175-cm flasks. If available, the remaining cells were centrifuged and washed in PBS, and the cell pellets were frozen. Again, at least 1000 cells per sgRNA were maintained under BVdU selection.

On day 25, all remaining cells were collected and counted. The remaining cells were divided in aliquots of 6×10^6 cells (which corresponds to 1000 cells per sgRNA) and washed in PBS, and the cell pellets were frozen for genomic DNA isolation for the final time point after BVdU selection. The screen was performed in two biological replicates.

Following completion of the screen, genomic DNA was isolated using a Qiagen Genomic DNA midi prep kit (catalog no. 51185) according to the manufacturer's protocol. Raw Illumina reads were normalized between samples using $\log_2[(\text{sgRNA reads/total reads for sample}) \times 1 \times 10^6 + 1]$. The initial time point data (day 10) were then subtracted from the end time point after BVdU selection (day 25) to determine the relative enrichment of each individual sgRNA after BVdU treatment using hypergeometric analysis and the STARS algorithm. A q value cutoff of <0.25 was used to call hits. The averaged data from two biological replicates were used for all analyses.

FACS-based TdTomato-GFP competition assay

293FT cells stably transduced with bicistronic lentiviruses encoding (i) DCK*-IKZF1 and GFP and (ii) DCK* and TdTomato were mixed together at a ratio of 1:99. Pooled cells were plated at a density of 20,000 cells per well of a six-well plate and in a total volume of 2 ml of media. Cells received 0.5 ml of the 6 μM POM stock solution to achieve an eventual final concentration of 1 μM or 0.5 ml of control media. The next day, the cells received 0.5 ml of 600 μM BVdU stock solution or 0.5 ml of control media. Cells were collected for

FACS analysis on days 0, 3, 6, 10, and 14. After each time point, cells were reseeded at 20,000 cells per well and treated with fresh BVdU (or DMSO).

FACS-based mCherry-BFP competition assay

DCK*-IKZF1 293FT cells were infected with a mixture of two lentiviruses encoding Cas9 and either (i) sgDCK and mCherry or (ii) sgCTRL and BFP (blue fluorescent protein). The two lentiviruses were mixed together such that the ratio of mCherry-positive to BFP-positive cells after infection and puromycin selection was 1:99. An analogous experiment was set up using a lentivirus encoding sgCTRL and mCherry. The pool of infected cells was plated at 20,000 cells per well in a six-well plate and then cultured in media containing either 100 μM BVdU or DMSO for 21 days. Cells were collected for FACS analysis on days 1, 6, 18, and 33. After each time point, cells were reseeded at 20,000 cells per well and treated with fresh BVdU.

Jurkat cells that had been stably infected to express Cas9 and DCK*-FOXP3 were superinfected with lentivirus encoding either (i) sgDCK and mCherry or (ii) sgCTRL and BFP. These cells were mixed together and analyzed by FACS to achieve a final ratio of mCherry-positive to BFP-positive cells of 1:99. The pool of infected cells was plated at 40,000 cells/ml in a six-well plate and then cultured in media containing either 100 μM BVdU or DMSO for 14 days. Cells were collected for FACS analysis on days 6 and 14.

The Jurkat cells expressing Cas9 and ASCL1-DCK* that were used for the CRISPR-Cas9 screen described above were superinfected with lentiviruses encoding sgRNAs targeting *CDK2*, *ASCL1*, or a nontargeting sgRNA as a control, the fluorescent protein mCherry and a puromycin resistance gene or with a lentivirus encoding a nontargeting sgRNA as a control, and the fluorescent protein BFP and a puromycin resistance gene (see schema in fig. S16F). The cells were selected with puromycin. mCherry puromycin-resistant cells were then mixed with BFP puromycin-resistant cells at a 1:3 ratio as determined by FACS analysis. The mixed cells were plated at 5×10^4 cells/ml and then cultured in media containing 500 μM BVdU or DMSO (0) for 18 days. FACS analysis was performed every 6 days. After each FACS analysis, fresh BVdU was added, and the density of the cells was adjusted to 5×10^4 cells/ml with fresh media.

CDK2 degrader drug treatments and cycloheximide chase experiments

Cells were counted using a Vi-Cell XR cell counter and were plated at a concentration of 4×10^5 cells/ml per well for NCI-H1092, 188, and 97-2 SCLC cell lines or at 1×10^6 cells/ml per well for the NCI-H1876 SCLC cell line in six-well plates. Cells were then treated with the CDK2 degraders TMX-2138, TMX-2172, or the negative degrader ZXH-7035 (Neg Deg) at 500 nM for 36 hours for NCI-H1092 and NCI-H1876 human SCLC cell lines or 8 hours for 188 and 97-2 mouse SCLC cell lines. For half-life time determination with cycloheximide, 97-2 cells were treated with CDK2 degraders for 4 hours before the addition of cycloheximide at 150 μg/ml. Cells were harvested at the indicated times after addition of cycloheximide.

Real-time RT-qPCR

293FT cells were seeded in six-well plates at a density of 750,000 cells per well in 2.5 ml of media per well. The next day, the cells were treated with the indicated concentrations of Spautin-1, POM, or DMSO for 24 hours. Multiple myeloma cells were seeded in 10-cm plates at a density of 0.75×10^6 cells/ml in a total volume of 9 ml of media. The next day, the cells were treated with the indicated concentrations of Spautin-1, POM, or DMSO. RNA was extracted using an RNeasy mini kit (Qiagen, #74106) according to the manufacturer's instructions. RNA concentration was determined using the NanoDrop 8000 (Thermo Fisher Scientific). cDNA was generated by reverse transcription using the AffinityScript qPCR (quantitative PCR) cDNA Synthesis kit (Agilent, 600559) according to the manufacturer's instructions. qPCR was performed using the LightCycler 480 (Roche) with the LightCycler 480 Probes Master Kit (Roche) and TaqMan probes (Thermo Fisher Scientific) according to the manufacturer's instructions. The Ct values for each probe were then normalized to the Ct value of ACTB for that sample. The data from each experiment were then normalized to the control to determine the relative fold change in mRNA expression. The following TaqMan probes were used: Hs00958474_m1 (IKZF1 human), ASCL1 human Hs04187546_g1 for detection of endogenous ASCL1, ASCL1 human Hs05000540_s1 for detection of the exogenous ASCL1-DCK* fusion, ACTB human Hs01060665_m1, Ascl1 mouse Mm03058063_m1, and Actb mouse Mm00607939_s1. All quantitative calculations were performed using the $2^{-\Delta\Delta Ct}$ method using *Beta Actin* (*ACTB*) as a reference gene.

Statistical analysis

For the positive selection small-molecule screen, GFP fluorescence for each well was normalized to untreated wells. For each library drug, normalized GFP fluorescence was plotted as a function of library drug concentration. Each drug treatment was performed in duplicate. Data were analyzed and plotted using GraphPad Prism v6, median inhibitory concentration (IC_{50}) values were determined using the "log (inhibitor) versus response -- Variable slope (four parameters)" analysis module, and area under the curve (AUC) values were determined using the "AUC" analysis module (*13*). For the positive selection CRISPR-Cas9 BVdU resistance screen, the relative fold enrichment of each individual sgRNA after BVdU treatment was calculated using both Broad Institute's hypergeometric analysis and the STARS algorithm to determine a rank list of candidate ASCL1 stabilizer genes ranked by q value, where statistical significance is $q < 0.25$.

For all other experiments, statistical significance was calculated using unpaired, two-tailed Student's t test. P values were considered statistically significant if the P value was <0.05. For all figures, $^*P < 0.05$, $^{**}P < 0.01$, $^{***}P < 0.001$, and $^{****}P < 0.0001$. Error bars represent SD unless otherwise indicated.

SUPPLEMENTARY MATERIALS

Supplementary material for this article is available at http://advances.sciencemag.org/cgi/content/full/7/6/eabd6263/DC1

REFERENCES AND NOTES

1. J. Krönke, N. D. Udeshi, A. Narla, P. Grauman, S. N. Hurst, M. M. Conkey, T. Svinkina, D. Heckl, E. Comer, X. Li, C. Ciarlo, E. Hartman, N. Munshi, M. Schenone, S. L. Schreiber, S. A. Carr, B. L. Ebert, Lenalidomide causes selective degradation of IKZF1 and IKZF3 in multiple myeloma cells. *Science* **343**, 301–305 (2014).
2. G. Lu, R. E. Middleton, H. Sun, M. V. Naniong, C. J. Ott, C. S. Mitsiades, K.-K. Wong, J. E. Bradner, W. G. Kaelin Jr., The myeloma drug lenalidomide promotes the cereblon-dependent destruction of Ikaros proteins. *Science* **343**, 305–309 (2014).
3. W. G. Kaelin Jr., Common pitfalls in preclinical cancer target validation. *Nat. Rev. Cancer* **17**, 441–450 (2017).
4. A. Neschadim, J. C. M. Wang, T. Sato, D. H. Fowler, A. Lavie, J. A. Medin, Cell fate control gene therapy based on engineered variants of human deoxycytidine kinase. *Mol. Ther.* **20**, 1002–1013 (2012).

5. A. K. Gandhi, J. Kang, C. G. Havens, T. Conklin, Y. Ning, L. Wu, T. Ito, H. Ando, M. F. Waldman, A. Thakurta, A. Klippel, H. Handa, T. O. Daniel, P. H. Schafer, R. Chopra, Immunomodulatory agents lenalidomide and pomalidomide co-stimulate T cells by inducing degradation of T cell repressors Ikaros and Aiolos via modulation of the E3 ubiquitin ligase complex $CRL4^{CRBN}$. *Br. J. Haematol.* **164**, 811–821 (2014).
6. E. Bastida, J. del Prado, L. Almirall, G. A. Jamieson, A. Ordinas, Inhibitory effects of dipyridamole on growth, nucleoside incorporation, and platelet-activating capability in the U87MG and SKNMC human tumor cell lines. *Cancer Res.* **45**, 4048–4052 (1985).
7. D. R. Newell, P. M. O'Connor, A. H. Calvert, K. R. Harrap, The effect of the nucleoside transport inhibitor dipyridamole on the incorporation of [^{3}H]thymidine in the rat. *Biochem. Pharmacol.* **35**, 3871–3877 (1986).
8. S. J. Boyer, J. Burke, X. Guo, T. M. Kirrane, R. J. Snow, Y. Zhang, C. Sarko, L. Soleymanzadeh, A. Swinamer, J. Westbrook, F. DiCapua, A. Padyana, D. Cogan, A. Gao, Z. Xiong, J. B. Madwed, M. Kashem, S. Kugler, M. M. O'Neill, Indole RSK inhibitors. Part 1: Discovery and initial SAR. *Bioorg. Med. Chem. Lett.* **22**, 733–737 (2012).
9. T. M. Kirrane, S. J. Boyer, J. Burke, X. Guo, R. J. Snow, L. Soleymanzadeh, A. Swinamer, Y. Zhang, J. B. Madwed, M. Kashem, S. Kugler, M. M. O'Neill, Indole RSK inhibitors. Part 2: Optimization of cell potency and kinase selectivity. *Bioorg. Med. Chem. Lett.* **22**, 738–742 (2012).
10. P. P. Roux, D. Shahbazian, H. Vu, M. K. Holz, M. S. Cohen, J. Taunton, N. Sonenberg, J. Blenis, RAS/ERK signaling promotes site-specific ribosomal protein S6 phosphorylation via RSK and stimulates cap-dependent translation. *J. Biol. Chem.* **282**, 14056–14064 (2007).
11. D. W. Rasco, K. P. Papadopoulos, M. Pourdehnad, A. K. Gandhi, P. R. Hagner, Y. Li, X. Wei, R. Chopra, K. Hege, J. D. Martino, K. Shih, A first-in-human study of novel cereblon modulator avadomide (CC-122) in advanced malignancies. *Clin. Cancer Res.* **25**, 90–98 (2019).
12. G. M. Burslem, P. Ottis, S. Jaime-Figueroa, A. Morgan, P. M. Cromm, M. Toure, C. M. Crews, Efficient synthesis of immunomodulatory drug analogues enables exploration of structure-degradation relationships. *ChemMedChem* **13**, 1508–1512 (2018).
13. I. S. Harris, J. E. Endress, J. L. Coloff, L. M. Selfors, S. K. McBrayer, J. M. Rosenbluth, N. Takahashi, S. Dhakal, V. Koduri, M. G. Oser, N. J. Schauer, L. M. Doherty, A. L. Hong, Y. P. Kang, S. T. Younger, J. G. Doench, W. C. Hahn, S. J. Buhrlage, G. M. De Nicola, W. G. Kaelin Jr., J. S. Brugge, Deubiquitinases maintain protein homeostasis and survival of cancer cells upon glutathione depletion. *Cell Metab.* **29**, 1166–1181.e6 (2019).
14. J. Liu, H. Xia, M. Kim, L. Xu, Y. Li, L. Zhang, Y. Cai, H. V. Norberg, T. Zhang, T. Furuya, M. Jin, Z. Zhu, H. Wang, J. Yu, Y. Li, Y. Hao, A. Choi, H. Ke, D. Ma, J. Yuan, Beclin1 controls the levels of p53 by regulating the deubiquitination activity of USP10 and USP13. *Cell* **147**, 223–234 (2011).
15. Q. L. Sievers, G. Petzold, R. D. Bunker, A. Renneville, M. Słabicki, B. J. Liddicoat, W. Abdulrahman, T. Mikkelsen, B. L. Ebert, N. H. Thomä, Defining the human C2H2 zinc finger degrome targeted by thalidomide analogs through CRBN. *Science* **362**, eaat0572 (2018).
16. V. Koduri, S. K. McBrayer, E. Liberzon, A. C. Wang, K. J. Briggs, H. Cho, W. G. Kaelin Jr., Peptidic degron for IMiD-induced degradation of heterologous proteins. *Proc. Natl. Acad. Sci. U.S.A.* **116**, 2539–2544 (2019).
17. M. G. Oser, A. H. Sabet, W. Gao, A. A. Chakraborty, A. C. Schinzel, R. B. Jennings, R. Fonseca, D. M. Bonal, M. A. Booker, A. Flaifel, J. S. Novak, C. L. Christensen, H. Zhang, Z. T. Herbert, M. Y. Tolstorukov, E. J. Buss, K.-K. Wong, R. T. Bronson, Q.-D. Nguyen, S. Signoretti, W. G. Kaelin Jr., The KDM5A/RBP2 histone demethylase represses NOTCH signaling to sustain neuroendocrine differentiation and promote small cell lung cancer tumorigenesis. *Genes Dev.* **33**, 1718–1738 (2019).
18. A. Augustyn, M. Borromeo, T. Wang, J. Fujimoto, C. Shao, P. D. Dospoy, V. Lee, C. Tan, J. P. Sullivan, J. E. Larsen, L. Girard, C. Behrens, I. I. Wistuba, Y. Xie, M. H. Cobb, A. F. Gazdar, J. E. Johnson, J. D. Minna, ASCL1 is a lineage oncogene providing therapeutic targets for high-grade neuroendocrine lung cancers. *Proc. Natl. Acad. Sci. U.S.A.* **111**, 14788–14793 (2014).
19. M. D. Borromeo, T. K. Savage, R. K. Kollipara, M. He, A. Augustyn, J. K. Osborne, L. Girard, J. D. Minna, A. F. Gazdar, M. H. Cobb, J. E. Johnson, ASCL1 and NEUROD1 reveal heterogeneity in pulmonary neuroendocrine tumors and regulate distinct genetic programs. *Cell Rep.* **16**, 1259–1272 (2016).
20. B. Hu, J. Mitra, S. van den Heuvel, G. H. Enders, S and G2 phase roles for Cdk2 revealed by inducible expression of a dominant-negative mutant in human cells. *Mol. Cell. Biol.* **21**, 2755–2766 (2001).
21. S. van den Heuvel, E. Harlow, Distinct roles for cyclin-dependent kinases in cell cycle control. *Science* **262**, 2050–2054 (1993).
22. H. Zhu, L. Nie, C. G. Maki, Cdk2-dependent Inhibition of p21 stability via a C-terminal cyclin-binding motif. *J. Biol. Chem.* **280**, 29282–29288 (2005).
23. D. Parry, T. Guzi, F. Shanahan, N. Davis, D. Prabhavalkar, D. Wiswell, W. Seghezzi, K. Paruch, M. P. Dwyer, R. Doll, A. Nomeir, W. Windsor, T. Fischmann, Y. Wang, M. Oft, T. Chen, P. Kirschmeier, E. M. Lees, Dinaciclib (SCH 727965), a novel and potent cyclin-dependent kinase inhibitor. *Mol. Cancer Ther.* **9**, 2344–2353 (2010).
24. G. P. Gregory, S. J. Hogg, L. M. Kats, E. Vidacs, A. J. Baker, O. Gilan, M. Lefebure, B. P. Martin, M. A. Dawson, R. W. Johnstone, J. Shortt, CDK9 inhibition by dinaciclib potently suppresses Mcl-1 to induce durable apoptotic responses in aggressive MYC-driven B-cell lymphoma in vivo. *Leukemia* **29**, 1437–1441 (2015).
25. M. Teng, J. Jiang, Z. He, N. P. Kwiatkowski, K. A. Donovan, C. E. Mills, C. Victor, J. M. Hatcher, E. S. Fischer, P. K. Sorger, T. Zhang, N. S. Gray, Development of CDK2 and CDK5 dual degrader TMX-2172. *Angew. Chem. Int. Ed. Engl.* **59**, 13865–13870 (2020).
26. A. Lopez-Girona, D. Mendy, T. Ito, K. Miller, A. K. Gandhi, J. Kang, S. Karasawa, G. Carmel, P. Jackson, M. Abbasian, A. Mahmoudi, B. Cathers, E. Rychak, S. Gaidarova, R. Chen, P. H. Schafer, H. Handa, T. O. Daniel, J. F. Evans, R. Chopra, Cereblon is a direct protein target for immunomodulatory and antiproliferative activities of lenalidomide and pomalidomide. *Leukemia* **26**, 2326–2335 (2012).
27. Y. X. Zhu, E. Braggio, C.-X. Shi, L. A. Bruins, J. E. Schmidt, S. Van Wier, X.-B. Chang, C. C. Bjorklund, R. Fonseca, P. L. Bergsagel, R. Z. Orlowski, A. K. Stewart, Cereblon expression is required for the antimyeloma activity of lenalidomide and pomalidomide. *Blood* **118**, 4771–4779 (2011).
28. L.-H. Zhang, J. Kosek, M. Wang, C. Heise, P. H. Schafer, R. Chopra, Lenalidomide efficacy in activated B-cell-like subtype diffuse large B-cell lymphoma is dependent upon IRF4 and cereblon expression. *Br. J. Haematol.* **160**, 487–502 (2013).
29. M. Kasim, V. Heß, H. Scholz, P. B. Persson, M. Fähling, Achaete-scute homolog 1 expression controls cellular differentiation of neuroblastoma. *Front. Mol. Neurosci.* **9**, 156 (2016).
30. F. R. Ali, K. Cheng, P. Kirwan, S. Metcalfe, F. J. Livesey, R. A. Barker, A. Philpott, The phosphorylation status of Ascl1 is a key determinant of neuronal differentiation and maturation in vivo and in vitro. *Development* **141**, 2216–2224 (2014).
31. L. A. Wylie, L. J. Hardwick, T. D. Papkovskaia, C. J. Thiele, A. Philpott, Ascl1 phospho-status regulates neuronal differentiation in a *Xenopus* developmental model of neuroblastoma. *Dis. Model. Mech.* **8**, 429–441 (2015).
32. Z. Chen, Z. Wang, J. C. Pang, Y. Yu, S. Bieerkehazhi, J. Lu, T. Hu, Y. Zhao, X. Xu, H. Zhang, J. S. Yi, S. Liu, J. Yang, Multiple CDK inhibitor dinaciclib suppresses neuroblastoma growth via inhibiting CDK2 and CDK9 activity. *Sci. Rep.* **6**, 29090 (2016).
33. M. E. M. Dolman, E. Poon, M. E. Ebus, I. J. M. den Hartog, C. J. M. van Noesel, Y. Jamin, A. Hallsworth, S. P. Robinson, K. Petrie, R. W. Sparidans, R. J. Kok, R. Versteeg, H. N. Caron, L. Chesler, J. J. Molenaar, Cyclin-dependent kinase inhibitor AT7519 as a potential drug for MYCN-dependent neuroblastoma. *Clin. Cancer Res.* **21**, 5100–5109 (2015).
34. J. J. Molenaar, M. E. Ebus, D. Geerts, J. Koster, F. Lamers, L. J. Valentijn, E. M. Westerhout, R. Versteeg, H. N. Caron, Inactivation of CDK2 is synthetically lethal to MYCN over-expressing cancer cells. *Proc. Natl. Acad. Sci. U.S.A.* **106**, 12968–12973 (2009).
35. T. Matsuo, P. Seth, C. J. Thiele, Increased expression of p27Kip1 arrests neuroblastoma cell growth. *Med. Pediatr. Oncol.* **36**, 97–99 (2001).
36. O. Kranenburg, V. Scharnhorst, A. J. Van der Eb, A. Zantema, Inhibition of cyclin-dependent kinase activity triggers neuronal differentiation of mouse neuroblastoma cells. *J. Cell Biol.* **131**, 227–234 (1995).
37. A. Borriello, V. Cucciolla, M. Criscuolo, S. Indaco, A. Oliva, A. Giovane, D. Bencivenga, A. Iolascon, V. Zappia, F. D. Ragione, Retinoic acid induces $p27^{Kip1}$ nuclear accumulation by modulating its phosphorylation. *Cancer Res.* **66**, 4240–4248 (2006).
38. G. M. Burslem, C. M. Crews, Proteolysis-targeting chimeras as therapeutics and tools for biological discovery. *Cell* **181**, 102–114 (2020).
39. J. G. Doench, E. Hartenian, D. B. Graham, Z. Tothova, M. Hegde, I. Smith, M. Sullender, B. L. Ebert, R. J. Xavier, D. E. Root, Rational design of highly active sgRNAs for CRISPR-Cas9–mediated gene inactivation. *Nat. Biotechnol.* **32**, 1262–1267 (2014).
40. Z. U, S. Hintermann, K. Hurth, S. Jacquier, H. Lehmann, H. Moebitz, N. Soldermann, A. Stojanovic, WO2015010641 – Substituted quinazolin-4-one derivatives, PCT/CN2014/082946, US Patent Office (Granted 12/12/2017).
41. The ORFeome Collaboration, The ORFeome Collaboration: A genome-scale human ORF-clone resource. *Nat. Methods* **13**, 191–192 (2016).
42. M. G. Oser, R. Fonseca, A. A. Chakraborty, R. Brough, A. Spektor, R. B. Jennings, A. Flaifel, J. S. Novak, A. Gulati, E. Buss, S. T. Younger, S. K. Mc Brayer, G. S. Cowley, D. M. Bonal, Q.-D. Nguyen, L. Brulle-Soumare, P. Taylor, S. Cairo, C. J. Ryan, E. J. Pease, K. Maratea, J. Travers, D. E. Root, S. Signoretti, D. Pellman, S. Ashton, C. J. Lord, S. T. Barry, W. G. Kaelin Jr., Cells lacking the *RB1* tumor suppressor gene are hyperdependent on aurora B kinase for survival. *Cancer Discov.* **9**, 230–247 (2019).
43. M. Abu-Remaileh, G. A. Wyant, C. Kim, N. N. Laqtom, M. Abbasi, S. H. Chan, E. Freinkman, D. M. Sabatini, Lysosomal metabolomics reveals V-ATPase- and mTOR-dependent regulation of amino acid efflux from lysosomes. *Science* **358**, 807–813 (2017).
44. T. Wang, K. Birsoy, N. W. Hughes, K. M. Krupczak, Y. Post, J. J. Wei, E. S. Lander, D. M. Sabatini, Identification and characterization of essential genes in the human genome. *Science* **350**, 1096–1101 (2015).
45. H.-T. Huang, D. Dobrovolsky, J. Paulk, G. Yang, E. L. Weisberg, Z. M. Doctor, D. L. Buckley, J.-H. Cho, E. Ko, J. Jang, K. Shi, H. G. Choi, J. D. Griffin, Y. Li, S. P. Treon, E. S. Fischer, J. E. Bradner, L. Tan, N. S. Gray, A chemoproteomic approach to query the degradable kinome using a multi-kinase degrader. *Cell Chem. Biol.* **25**, 88–99.e6 (2018).

46. B. Nabet, J. M. Roberts, D. L. Buckley, J. Paulk, S. Dastjerdi, A. Yang, A. L. Leggett, M. A. Erb, M. A. Lawlor, A. Souza, T. G. Scott, S. Vittori, J. A. Perry, J. Qi, G. E. Winter, K.-K. Wong, N. S. Gray, J. E. Bradner, The dTAG system for immediate and target-specific protein degradation. *Nat. Chem. Biol.* **14**, 431–441 (2018).
47. J. Navarrete-Perea, Q. Yu, S. P. Gygi, J. A. Paulo, Streamlined tandem mass tag (SL-TMT) protocol: An efficient strategy for quantitative (phospho)proteome profiling using tandem mass tag-synchronous precursor selection-MS3. *J. Proteome Res.* **17**, 2226–2236 (2018).
48. J. P. Gygi, R. Rad, J. Navarrete-Perea, S. Younesi, S. P. Gygi, J. A. Paulo, A triple knockout isobaric-labeling quality control platform with an integrated online database search. *J. Am. Soc. Mass Spectrom.* **31**, 1344–1349 (2020).
49. G. C. McAlister, E. L. Huttlin, W. Haas, L. Ting, M. P. Jedrychowski, J. C. Rogers, K. Kuhn, I. Pike, R. A. Grothe, J. D. Blethrow, S. P. Gygi, Increasing the multiplexing capacity of TMTs using reporter ion isotopologues with isobaric masses. *Anal. Chem.* **84**, 7469–7478 (2012).
50. M. E. Ritchie, B. Phipson, D. Wu, Y. Hu, C. W. Law, W. Shi, G. K. Smyth, limma powers differential expression analyses for RNA-sequencing and microarray studies. *Nucleic Acids Res.* **43**, e47 (2015).

Acknowledgments: We thank the members of the Kaelin and Oser laboratories for helpful discussions. Special thanks to the ICCB (Longwood) at HMS for assistance with small-molecule screens, to W. Gao for generation of adenoviral vectors used for recombination cloning, and D. Hong for generation of SCLC mouse cell lines. **Funding:** W.G.K. is supported by an NIH R35 grant and is an HHMI investigator. M.G.O. is supported by a Damon Runyon Cancer Research Foundation Clinical Investigator Award and an NCI/NIH KO8 grant (no. K08CA222657). V.K. is supported by an American Society of Hematology Research Training Award and T32 NIH Training Grant CA009172. J.A.P. is funded by an NIGMS grant R01 GM132129. E.S.F. is funded by NCI R01CA2144608. N.S.G. is funded by NIH R01 CA214608-03. M.I. is supported by an Internationalisation Fellowship from the Carlsberg Foundation. C.J.O. is supported by an NIH/NCI Pathway to Independence Award (R00CA190861). **Author contributions:** V.K., L.D., and B.L.L. performed experiments and, together with W.G.K. and M.G.O., designed experiments, analyzed data, and assembled and wrote the manuscript. J.A.M. helped design experiments. A.C.W. and A.H.S. performed experiments. M.I. designed and synthesized the IMiD library. J.P. and C.J.O. measured CRBN binding and cellular activity of candidate IMiDs; J.B. supervised these experiments. I.S.H. and J.E.E. constructed the Ludwig anticancer and antimetabolite libraries and helped analyze data from the screen. E.D., X.L., and S.J.B. synthesized and characterized Spautin-1 derivatives. J.A.P. performed TMT global proteomic profiling of Spautin-1. S.P.G. supervised these experiments. K.A.D. and E.S.F. analyzed TMT proteomic data. K.J.B. determined the half-lives of luciferase fusion proteins and the Z′ of the dual-luciferase system. J.G.D. helped analyze data from the CRISPR screen. M.T., T.Z., and N.S.G. helped generate and validate CDK2 degraders. **Competing interests:** W.G.K. has financial interests in Lilly Pharmaceuticals, Fibrogen, Agios Pharmaceuticals, Cedilla Therapeutics, Nextech Invest, Tango Therapeutics, and Tracon Pharmaceuticals. N.S.G. is a founder, science advisory board member, and equity holder in Gatekeeper, Syros, Petra, C4, B2S, Aduro, and Soltego (board member). E.S.F. is a founder, scientific advisory board (SAB) member, and equity holder of Civetta Therapeutics, Jengu Therapeutics (board member), and Neomorph Inc. E.S.F. is an equity holder of C4 Therapeutics. E.S.F. consults or has consulted for Novartis, AbbVie, Astellas, Deerfield, EcoR1, and Pfizer. The Fischer laboratory receives or has received research funding from Novartis, Deerfield, and Astellas. The Gray laboratory receives or has received research funding from Novartis, Takeda, Astellas, Taiho, Janssen, Kinogen, Voronoi, Her2llc, Deerfield, and Sanofi. M.G.O. has sponsored research agreements with Lilly Pharmaceuticals and Takeda Pharmaceuticals. V.K. has consulted for Cedilla Therapeutics. S.J.B. is on the SAB of Adenoid Cystic Carcinoma Foundation. J.B. is an employee, executive, and shareholder of Novartis AG (Basel, Switzerland). J.G.D. consults for Agios, Foghorn Therapeutics, Maze Therapeutics, Merck, and Pfizer; J.G.D. consults for and has equity in Tango Therapeutics. J.G.D.'s interests were reviewed and are managed by the Broad Institute in accordance with its conflict of interest policies. I.S.H. is a consultant for ONO Pharmaceuticals (USA). V.K. and W.G.K. are inventors on a patent application on positive selection assays to identify protein degraders, which was filed by the Dana-Farber Cancer Institute (U.S. patent application number 16/332,921, filed on 13 March 2019 and published on 1 August 2019). N.S.G., M.T., and T.Z. are named inventors on patent applications covering Cdlk2 degraders described in the paper, and which were filed by the Dana Farber Cancer Institute (U.S. Provisional Application No. 62/829,302, filed April 4, 2019 and U.S. Provisional Application No: 62/981,334, filed February 25, 2020). The authors declare that they have no other competing interests. **Data and materials availability:** All data needed to evaluate the conclusions in the paper are present in the paper and/or the Supplementary Materials. Additional data related to this paper may be requested from the authors. All plasmids are available from the authors.

Submitted 2 July 2020
Accepted 17 December 2020
Published 5 February 2021
10.1126/sciadv.abd6263

Citation: V. Koduri, L. Duplaquet, B. L. Lampson, A. C. Wang, A. H. Sabet, M. Ishoey, J. Paulk, M. Teng, I. S. Harris, J. E. Endress, X. Liu, E. Dasilva, J. A. Paulo, K. J. Briggs, J. G. Doench, C. J. Ott, T. Zhang, K. A. Donovan, E. S. Fischer, S. P. Gygi, N. S. Gray, J. Bradner, J. A. Medin, S. J. Buhrlage, M. G. Oser, W. G. Kaelin Jr., Targeting oncoproteins with a positive selection assay for protein degraders. *Sci. Adv.* **7**, eabd6263 (2021).